FEBS Letters

FEBS PRESS
science publishing by scientists

EDITOR'S CHOICE

Defining the architecture of the human TIM22 complex by chemical crosslinking

Anusha Valpadashi[1], Sylvie Callegari[1,2,3], Andreas Linden[4,5], Piotr Neumann[6], Ralf Ficner[6,7], Henning Urlaub[4,5], Markus Deckers[1] and Peter Rehling[1,7,8]

1 Department of Cellular Biochemistry, University Medical Center Göttingen, Germany
2 Ubiquitin Signalling Division, The Walter and Eliza Hall Institute of Medical Research, Parkville, Australia
3 Department of Medical Biology, University of Melbourne, Australia
4 Bioanalytical Mass Spectrometry Group, Max Planck Institute for Biophysical Chemistry, Göttingen, Germany
5 Department of Clinical Chemistry, Bioanalytics, University Medical Center Göttingen, Germany
6 Department of Molecular Structural Biology, Institute for Microbiology and Genetics, Göttingen Center for Molecular Biosciences, Georg-August-University Göttingen, Germany
7 Cluster of Excellence "Multiscale Bioimaging: from Molecular Machines to Networks of Excitable Cells" (MBExC), University of Goettingen, Germany
8 Max Planck Institute for Biophysical Chemistry, Göttingen, Germany

Correspondence
P. Rehling, Department of Cellular Biochemistry, University Medical Center Göttingen, Humboldtallee 23, Göttingen 37073, Germany
Tel: +49 551 395947
E-mail: peter.rehling@medizin.uni-goettingen.de

Anusha Valpadashi and Sylvie Callegari contributed equally to this study

(Received 15 September 2020, revised 19 October 2020, accepted 25 October 2020, available online 13 November 2020)

doi:10.1002/1873-3468.13978

Edited by Peter Brzezinski

The majority of mitochondrial proteins are nuclear encoded and imported into mitochondria as precursor proteins *via* dedicated translocases. The translocase of the inner membrane 22 (TIM22) is a multisubunit molecular machine specialized for the translocation of hydrophobic, multi-transmembrane-spanning proteins with internal targeting signals into the inner mitochondrial membrane. Here, we undertook a crosslinking-mass spectrometry (XL-MS) approach to determine the molecular arrangement of subunits of the human TIM22 complex. Crosslinking of the isolated TIM22 complex using the BS3 crosslinker resulted in the broad generation of crosslinks across the majority of TIM22 components, including the small TIM chaperone complex. The crosslinking data uncovered several unexpected features, opening new avenues for a deeper investigation into the steps required for TIM22-mediated translocation in humans.

Keywords: carrier translocase; crosslinking-mass spectrometry; mitochondria; protein translocation; TIM22

The translocase of the inner membrane, TIM22 (carrier translocase), is responsible for the insertion of multi-transmembrane domain proteins with internal targeting signals into the inner mitochondrial membrane. Such proteins typically comprise of metabolite carriers or membrane-embedded components of the mitochondrial import machinery, and their function is essential for life [1–3]. Precursor substrates of the TIM22 pathway possess internal targeting signals that are recognized by receptor proteins on the translocase of the outer membrane (TOM complex) [4–8]. Upon translocation through the TOM complex, the precursor protein is bound by the small TIM chaperone complexes that maintain the precursor in an import-competent state, by preventing aggregation of the hydrophobic transmembrane segments. The precursor

Abbreviations
bRP, basic reversed-phase; PMSF, phenylmethylsulfonylfluoride; pSEC, peptide size exclusion chromatography; TFA, trifluoroacetic acid; TIM22, translocase of the inner membrane 22; TOM, translocase of the outer membrane.

This is an open access article under the terms of the Creative Commons Attribution-NonCommercial-NoDerivs License, which permits use and distribution in any medium, provided the original work is properly cited, the use is non-commercial and no modifications or adaptations are made.

is then shuttled across the aqueous intermembrane space to the TIM22 complex for insertion into the inner mitochondrial membrane [9–11].

Studies using yeast have shown that the conserved carrier translocase is composed of a core complex embedded into the inner membrane that includes a dual pore-forming unit generated by the Tim22 protein [12–14]. Associated membrane integrated subunits, Tim18, Tim54 and SdhA support complex assembly and provide structural integrity [15–19]. The core structural components of the human TIM22 complex have only been defined in recent years and were found to be largely divergent from the yeast complex. Aside from the TIM22 pore-forming unit, the human translocase contains only two metazoan-specific components; TIM29 and the acyl glycerol kinase, AGK [20–25]. The precise function of these metazoan-specific components within the complex remains unknown.

The family of small TIM proteins, so called due to their low molecular weight (from 8 to 12 kDa), are defined by a twin CX_3C zinc-finger motif that generates an intramolecular disulfide bond, enabling them to fold in a hairpin-like structure. Yeast has five soluble small TIM proteins, four of which can associate to make up hexameric ring structures comprising of either Tim9-Tim10, or Tim8-Tim13, each with different substrate specificities [9,26,27]. The fifth small TIM in yeast is TIM12, which mediates docking of the TIM9-TIM10 hexamer by integrating into the hexamer and associating it to the core complex *via* Tim54 [28,29]. Both hexameric complexes are conserved in human, although the human TIM8-TIM13 complex has not been found to associate with the translocase [20] and is dispensable for TIM22-mediated import [30]. Instead, it was shown that the two human isoforms of Tim8, TIM8A and TIM8B, have acquired novel cell-specific functions for complex IV assembly [30]. Humans also have two isoforms of TIM10, TIM10A and TIM10B [31,32]. TIM10A, like its yeast counterpart, forms a hexameric complex with TIM9 and is herein referred to simply as TIM10. In contrast, TIM10B remains constitutively associated with the core TIM22 complex and so it was proposed to be the functional human homolog of the yeast Tim12 protein, the docking site for the small TIM chaperone complex [31]. However, this was not functionally verified and it remains unclear how the small TIM chaperones bind to the core TIM22 complex and release their cargo.

Here, we undertook a chemical crosslinking approach coupled with mass spectrometry to map the spatial arrangement of the core human TIM22 complex, together with the small TIM chaperone complexes. This map elucidates key structural features of the complex, including contact sites for the small TIM chaperones and interaction sites for the TIM22 and TIM29 subunits. It furthermore reveals conformational flexibility within the helices of the small TIM chaperone complexes in human. Several disease-causing mutations have been discovered in the core TIM22 complex [33–37] and in the small TIM chaperones [38,39]. Therefore, this information not only provides an insight into the workings of the TIM22 complex, but is also crucial for understanding the molecular basis of disease-causing mutations.

Materials and methods

Cell culture

DMEM media (Gibco™, Thermo Fisher Scientific, Waltham, MA, USA) supplemented with 10% sterile filtered fetal bovine serum (Sigma, Saint Louis, MO, USA) was used to culture human embryonic kidney cell lines (HEK293T-Flp-In™ T-Rex™) at 37 °C with 5% CO_2. The generation of stably expressing C-terminally FLAG-tagged TIM29 inducible HEK293T cell line was previously described [40]

Antibodies

Primary antibodies were raised in rabbit (anti-AGK, anti-LETM, anti-ATP5B, [40]; anti-TIM9, [41]), or purchased (anti-TIM22, anti-TIM29, Proteintech, Rosemont, IL, USA; anti-LRPPRC, abcam, Cambridge, UK; anti-PRMT5, Cell Signalling Technology, Danvers, MA, USA; anti-FLAG, Sigma). Antibodies against TIM10A and TIM10B were raised in rabbit by immunization with C-terminal peptides of the individual proteins.

Mitochondrial isolation

Cells were harvested by centrifugation at 600 ***g*** for 10 min at 4 °C and washed with PBS (phosphate buffered saline). The cell pellet was resuspended in isolation buffer [300 mM Trehalose; 10 mM KCl; 10 mM HEPES, pH 7.4; 1 mM EDTA; 0.1%(w/v) BSA] containing freshly added 0.5 mM phenylmethylsulfonylfluoride (PMSF) and homogenized on ice using a Potter S Homogenizer (Sartorius, Goettingen, Germany). Homogenate was centrifuged at 800 ***g*** for 10 min at 4 °C to remove unbroken cells. Mitochondria were pelleted down at 12 000 ***g*** for 10 min at 4 °C and resuspended in isolation buffer without BSA. For protein estimation, Bradford assay was used with bovine serum albumin (BSA) as a standard.

FLAG immunoprecipitation

Mitochondria were solubilized in solubilization buffer [1% Digitonin; 20 mM Tris/HCL, pH 7.4; 100 mM NaCl;

0.5 mM EDTA; 20% (w/v) glycerol; 1 mM 1mM PMSF and 1× Roche (Basel, Switzerland) cOmplete™, EDTA-free Protease Inhibitor Cocktail] at a ratio of 1 mg·mL^{-1} and incubated on an end-over-end shaker for 20 min at 4 °C. For XL-MS experiments, 100 mg of isolated mitochondria was used as starting material. For the sample with RNase A treatment, 5 μg·mL^{-1} RNase A (Thermo Fisher Scientific) was added to the solubilization buffer. The mitochondrial suspension was centrifuged at 14 000 ***g*** for 10 min at 4 °C to pellet down unsolubilized mitochondria. Supernatant was added to the anti-FLAG agarose affinity resin (Sigma-Aldrich, Saint Louis, MO, USA) and incubated for 1 h at 4 °C on an end-over-end shaker. Unbound lysate was removed by centrifugation (100 ***g*** for 30 s at 4 °C) using filtered columns (Mobicols, MoBiTec GmbH, Goettingen, Germany) and the FLAG resin collected in the column was washed 10× with wash buffer [0.3% Digitonin; 20 mM Tris/HCl, pH 7.4; 100 mM NaCl; 0.5 mM EDTA and 20% (w/v) glycerol]. For native elution of TIM29^{FLAG}, 5 μg·mL^{-1} FLAG peptide (Sigma) with wash buffer was used for elution at 4 °C for 30 min on thermoshaker. For immunoblotting, 10–18% Tris-Tricine gels were used for protein separation. For Colloidal Coomassie staining, gels were incubated overnight with Colloidal Coomassie staining solution (ROTI®Blue Quick, Carl Roth, Karlsruhe, Germany) and washed with 1% acetic acid before scanning.

BS3 (bis(sulfosuccinimidyl)suberate) crosslinking

For crosslinking experiments, 1 M HEPES pH 7.4 was used instead of 1 M Tris/HCl pH 7.4 to prepare all buffers. After FLAG immunoprecipitation, the concentrated eluate was incubated for 2 h on ice with 2 or 5 mM BS3 crosslinker (Thermo Fisher Scientific) solubilized in wash buffer. An equal amount of wash buffer was added to the control. To quench the reaction, 125 mM of glycine (pH 8) was added and incubated on ice for 15 min. The sample was further used for immunoblotting or mass spectrometry analysis.

Protein digestion and enrichment of crosslinked peptides

Crosslinked proteins were reduced with 10 mM dithiothreitol and subsequently alkylated with 40 mM iodoacetamide. Digestion of proteins was performed using the SP3 paramagnetic bead processing approach [42,43], and the endoproteinase trypsin was used in a 1 : 50 enzyme-to-protein ratio at 37 °C overnight. The reaction was terminated with 0.5% trifluoroacetic acid (TFA) and peptides were desalted on MicroSpin Columns (Harvard Apparatus, Holliston, MA, USA) following manufacturer's instructions. Crosslinked peptides were either enriched by peptide size exclusion chromatography (pSEC) [44] or fractionated by basic reversed-phase (bRP) chromatography. For pSEC, dried peptides were resuspended in 50 μL 30% ACN/0.1% TFA (running buffer) and loaded onto a SuperdexPeptide 3.2/300 column operated by an ÄKTAmicro system (both GE Healthcare, Chicago, IL, USA). The flow rate was set to 50 μL·min^{-1}, and 50 μL fractions were collected. For bRP, desalted peptides were dissolved in 50 μL 10 mM NH_4OH pH 10. Peptides were loaded onto a Xbridge C18 column (Waters, Milford, MA, USA) using an Agilent 1100 series chromatography system (Agilent Technologies, Santa Clara, CA, USA). The column was operated at a flow rate of 60 μL·min^{-1} with a buffer system consisting of 10 mM NH_4OH pH 10 (buffer A) and 10 mM NH_4OH pH 10/80% [v/v] ACN (buffer B). The column was equilibrated with 5% B and developed over 64 min using the following gradient: 5% B (0–5 min), 5–10% B (5–8 min), 10–42% B (8–42 min), 42–60% B (42–50 min), 60–90% B (50–51 min), 90–95% B (51–56 min), 95–5% B (56–58 min), 5% B (58–64 min). The first 6 min were collected as one flow-through fraction, followed by 48 × 1 min fractions, which were reduced to 12 fractions by concatenated pooling. Fractionated peptides were vacuum dried, resuspended in 2% ACN/0.05% TFA, and subjected to LC-MS/MS analysis.

LC-MS/MS analysis

Peptides were measured in technical duplicates on a Q Exactive HF-X Mass Spectrometer coupled to a Dionex UltiMate 3000 UHPLC system (both Thermo Fisher Scientific) equipped with an in house-packed C18 column (ReproSil-Pur 120 C18-AQ, 1.9 μm pore size, 75 μm inner diameter, 30 cm length, Dr. Maisch GmbH, Ammerbuch, Germany). MS1 full scans were acquired in the orbitrap (OT) with a resolution of 120 000, an injection time (IT) of 60 ms and an automatic gain control (AGC) target of 1×10^6. Dynamic exclusion was set to 30 s and only charge states between 3 and 8 were considered for fragmentation. MS2 spectra were acquired in the OT of the 30 most abundant precursor ions; the resolution was set to 30 000; the IT to 128 ms and the AGC target to 1×10^5. Fragmentation was enforced by higher-energy collisional dissociation (HCD) at 30% NCE.

Data analysis

Raw files were analysed by PLINK 2 [45] (v. 2.3) for the identification of crosslinked peptides. Default settings were applied with carbamidomethylation of cysteine residues as fixed modification and oxidation of methionine residues as variable modification. BS3 was set as crosslinker. The global false discovery rate (FDR) was set to 5% at spectrum level. The protein databases contained either all identified proteins or the 1000 most abundant proteins based on the identification of linear peptides by MAXQUANT (v. 1.6.0.1) [46] and the respective iBAQ values. Crosslinking results were visualized by XINET [47].

Structural modelling

For the remodelling of the atomic model of Tim9-Tim10 complex, missing N- and C-terminal fragments of Tim9 and Tim10 entities comprising the crystal structure of human Tim9-Tim10 complex (PDB id: 2BSK) were modelled in COOT [48], based on the best resolved copy of Tim9 or Tim10 subunit in this structure. After the manual extension of missing fragments, the remodelled Tim9-Tim10 complex was subjected to all-atom energy-guided refinement in Rosetta force-field [49] (the relaxed protocol) utilizing positional constrains obtained from the starting model. During this step, missing side chain atoms in the deposited atomic model were restored.

Manual modelling of complexes was performed in PYMOL (http://www.pymol.org) and COOT based on spatial restraints derived from the crosslinking data. Figures were prepared using PYMOL.

Results and Discussion

Optimization of TIM22 complex isolation for BS3 crosslinking

Crosslinking coupled with mass spectrometry (XL-MS) has become a powerful approach in the study of multi-protein complexes, enabling not only the identification of crosslinked peptides, but also of the crosslinked residue. Based on a generated catalogue of crosslinked residues, protein composition within a complex can be mapped to provide an insight into the 3D arrangement of proteins within the complex [50,51]. We have previously shown that the TIM22 complex can be efficiently isolated *via* immunoprecipitation of TIM29^{FLAG} from HEK293T Flp-In cells that express inducible C-terminal FLAG-tagged TIM29 [40]. To exploit the use of XL-MS to obtain structural insights into TIM22 complex architecture, we upscaled this isolation approach to an amount that would enable the identification of crosslinks. Coomassie gel staining of the isolated complex revealed a number of protein components that co-isolated with TIM29^{FLAG} and subsequent MALDI mass spectrometry analysis of these bands (data not shown) verified that all known components of the TIM22 complex were present, including the hexameric small TIMs, TIM9 and TIM10A (Fig. 1A). This was further confirmed by western blotting using antisera for known TIM22 components (Fig. 1B). The isolation also revealed contaminating proteins, the mitochondrial leucine-rich PPR motif-containing protein LRPPRC, together with its binding partner the SRA stem-loop interacting RNA binding protein, SLIRP, as well as the arginine methyltransferase, PRMT5. These proteins were equally present in the FLAG isolate from wild-type cells indicating a non Tim22-specific interaction with the FLAG affinity column (Fig. 1A,B).

Initial crosslinking analyses identified a high tendency for crosslinks to form between LRPPRC and SLIRP (data not shown) and it was therefore thought that the high protein levels of contaminating LRPPRC could be hampering crosslinking efficiency within the TIM22 complex. Size exclusion chromatography was unsuccessful in separating LRPPRC as it forms a complex with SLIRP at approximately 250 kDa, which can also oligomerize [51,52]. LRPPRC is known to have a strong RNA binding propensity [51], therefore, to determine whether this property contributes to its stickiness to the FLAG affinity beads, we modified the isolation protocol to include treatment with ribonuclease A (RNase A) during the immunoprecipitation (Fig. 1C). Strikingly, coomassie stained gels of isolated TIM22 complex with RNase A treatment show a clear absence of detectable LRPPRC compared with the untreated sample (Fig. 1D). Western blotting confirmed the absence of both LRPPRC and SLIRP (Fig. 1E). RNase treatment did not affect the integrity of the TIM22 complex, with all components being present in the isolate (Fig. 1D,E) To more quantitatively verify that levels of the LRPPRC-SLIRP complex were diminished, mass spectrometry analysis was performed on samples treated with and without RNase A. Plotting of the intensities from Label Free Quantification (LFQ) of both samples showed a strong reduction of approximately 245-fold in LRPPRC levels upon treatment with RNase A (Fig. S1). The contaminant PRGT5 was still present, but since there were no crosslinks detected with PRGT5 in our initial analyses (data not shown), it was not expected to interfere with the crosslinking efficiency.

XL-MS analysis of human TIM22 complex using BS3

The water soluble, amine-amine bifunctional crosslinker, bis(sulfosuccinimidyl)suberate (BS3), has previously been successfully used for the XL-MS analysis of mitochondrial proteins [53]. BS3 has an arm length of 11.4 Å, providing a medium length range for crosslinking of TIM22 components. To test the suitability of BS3 for XL-MS analysis, isolated TIM22 complex was incubated with BS3 for two hours and crosslinking efficiency was analysed by SDS/PAGE and western blotting. Crosslinks, evident as slower migrating bands, were observed for all TIM22 components, confirming the suitability of BS3 for XL-MS analysis (Fig. 2A). Notably, TIM9 and TIM10 had

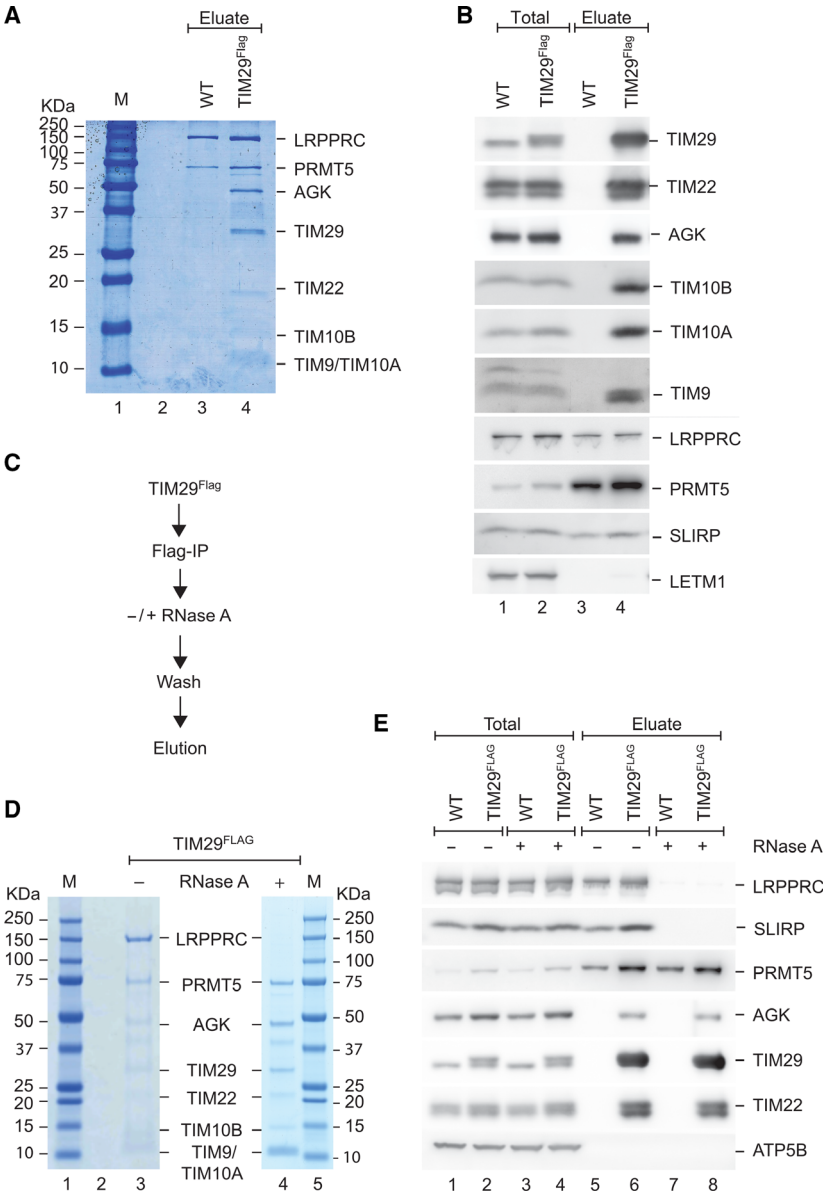

Fig. 1. Optimization of TIM22 complex isolation. (A) Mitochondria were isolated from wild-type (WT) and TIM29^{FLAG}HEK293T Flp-In cells. Isolated mitochondria were solubilized and subjected to FLAG immunoprecipitation. The eluate (100%) was analysed by SDS/PAGE, followed by coomassie blue staining. Bands were excised and analysed by LC/MS to verify protein identity. (B) Eluate from immunoprecipitation described in (A) was analysed by Tris-Tricine gel and immunoblotted with the respective protein antibodies. The mitochondrial inner membrane protein LETM1 was included as a negative control. 10% Total; 100% Eluate. (C) Schematic representation of experimental workflow for RNase A treatment. RNase A was added during the solubilization of the mitochondria for FLAG immunoprecipitation. (D) Isolated TIM22 complex from RNAse A-treated and non-treated samples was analysed by Tris-Glycine gel, followed by coomassie blue staining. (E) Isolated TIM22 complex described in (D) was analysed by Tris-Tricine gel and immunoblotted with the respective protein antibodies. The ATPase subunit ATP5B was included as a negative control. 10% Total; 100% Eluate.

almost identical crosslinking patterns, consistent with their expected co-assembly within the hexameric ring complex.

With the establishment of these crosslinking procedures, we proceeded with mass spectrometry analysis of the BS3 crosslinked TIM22 complex. Proteins were digested and crosslinked peptides were enriched using peptide size exclusion chromatography (pSEC). Fractions containing crosslinks were collected and analysed using LC-MS/MS and the PLINK 2 software was used for identification of crosslinked peptides. Two experimental replicates were performed. Results revealed a number of BS3-dependent intermolecular crosslinks. Intermolecular crosslinks between TIM22 complex components for each experiment are listed in Table S1A,B respectively and depicted in Fig. 2B. As expected, intermolecular crosslinks were detected between the TIM9 and TIM10 proteins, but also between the small TIMs and each of the core TIM22 components TIM29, TIM22 and AGK. Notably, crosslinks were also observed between the N-terminal matrix domain of TIM29 and the first matrix facing loop of TIM22 (Fig. 2B), suggesting an interaction interface between TIM22 and TIM29 within the matrix. Interestingly, one of the crosslinks with the matrix domain of TIM29 involves a conserved residue

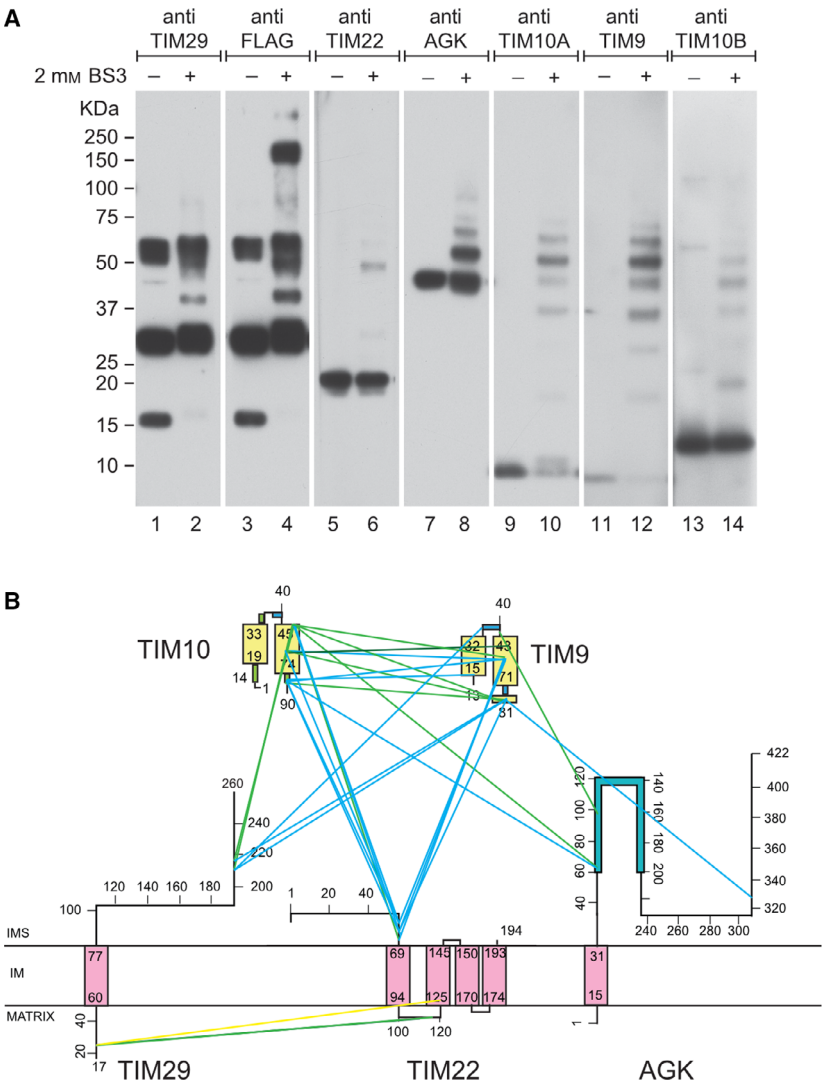

Fig. 2. BS3 crosslinking and MS analysis of human TIM22 complex (A) Isolated TIM22 complex was crosslinked with 2 mMof BS3 crosslinker. For control sample, water without crosslinker was added to the sample. 20% of the reaction volume was loaded for each lane and analysed by SDS/PAGE gel and immunoblotting with the respective antibodies. (B) Schematic showing intermolecular crosslinks identified by LC-MS/MS analysis without (yellow/green lines) and after (blue/green lines) RNAse A treatment. Numbers indicate protein residue. TM, transmembrane; IMS, intermembrane space; Teal: inter-crosslinks; Pink: transmembrane domain; Yellow: helix; Green: beta turn; Blue: beta bend; Turquoise: diacylglycerol Kinase catalytic domain (DAGKc).

of TIM22 (K127) which, in yeast, has been shown to be essential for the interaction of Tim22 with Tim18 [54]. This suggests that this is a functional interaction region and it could be that TIM29 in metazoa has structurally replaced the yeast Tim18. The matrix region TIM22-TIM29 crosslinks were the only crosslinks detected between the membrane integrated components of the complex, possibly reflecting a limitation of using a hydrophilic crosslinker. Nevertheless, the close positioning of these regions could mean that the matrix domains are important for complex assembly.

Crosslinks demonstrate conformational flexibility within the TIM9-TIM10 complex

Both TIM9 and TIM10 have a helix-loop-helix structure, which is maintained in a hairpin fold by twin disulfide bonds, as depicted in Fig. 2B. The crystal structure of both the *Saccharomyces cerevisiae* and human hexameric TIM9-TIM10 complexes have previously been solved to reveal a six-bladed α-propeller conformation made up of alternating molecules of TIM9 and TIM10 [32,55]. This hexameric structure has an ordered circular core with the loops making up one flat surface of the complex, whereas the other surface has amphiphilic tentacles, comprising of the N and C termini helices of TIM9 and TIM10, that protrude from the centre of the core [32,55]. To examine how the crosslinking data comply with the existing structure, we generated a model of the TIM9-TIM10 chaperone complex using the solved human structure (PDB id: 2BSK) [32]. Fragments of missing N or C termini were extended based on the best resolved copy of Tim9 or Tim10 subunits in this structure. The

completed model was refined in ROSETTA and missing side chain atoms in the deposited crystal structure were generated in order to visualize crosslinks (Fig. 3A,B).

Positioning of the intermolecular crosslinks onto the published model of the human chaperone complex reveals that a number of the crosslinks between TIM9 and TIM10 are not compatible with the 11.4 Å arm length of BS3 (Fig. 3C,D). One possibility is that these crosslinks form between two different small TIM hexamers. There is evidence that multiple small TIM hexamers interact with the precursor in a 'bead on a string' conformation to maintain the precursor in an elongated state [9], but it is unclear whether the hexamers would be in close enough proximity to form such extensive crosslinks.

Another possibility is that these crosslinks reflect the conformational flexibility of the C-terminal tentacles. A superimposition of the crystal structure of the yeast complex (PDB id: 3DXR) [55] over the human complex demonstrates the high degree of conservation between the two structures (Fig. S2). However, the superimposition also shows that the model of the yeast complex appears to have shorter tentacles, when in fact the N and C termini of yeast Tim9 and Tim10 are longer than in human. Thermal data and NMR experiments from the yeast Tim9-Tim10 complex showed the 12 protruding helices increase in mobility the further they extend from the core [9,55] and so the crystal structure of the yeast complex could not sufficiently resolve the N and C termini [55]. This is testament to the mobility of the tentacles, which is believed to be important for interaction with the precursor substrate. Of the crosslinks that met the distance criteria, these were primarily located towards the base of the complex, near the core region of the hexamer (TIM9-TIM10: K58-K81; K58-K45; K81-K68), consistent with the increased stability of this part of the complex (Fig. 3C,D). In contrast, crosslinks that involved the more outward protruding tentacles of TIM9 (TIM9-TIM10: K15-K81; K81-K81; K81-K45 and TIM9-TIM9: K58-K81) were less compliant with the distance criteria (Fig. 3C,D).

To further investigate conformational alterations resulting from helix flexibility, alternate models were generated to accommodate the required distance for two of the TIM9-TIM10 crosslink pairs; K15-K81 and K81–K81 (Fig. 3E–F and G–H, respectively). Each model relies on flexibility of the upper regions of the tentacles that correspond to the C-terminal regions of both Tim9 and Tim10.

Together, these data highlight the conformational flexibility of the upper tentacle regions of the small TIM chaperone complex. Interestingly, recent NMR data from the yeast chaperone complex indicate that mobility of the tentacles is maintained even upon binding of the precursor substrate [9] leading to the model that multiple dynamic conformations brought about by tentacle mobility can both enable tight binding of the precursor, as well as facilitate its subsequent release through a series of multiple weak interactions [9].

The TIM22 core complex has multiple interaction sites for the small TIM complex

Since the recent elucidation of the components of the human TIM22 complex, an outstanding question has been the docking site of the small TIM chaperone complex. BS3 crosslinking data revealed several prominent interaction interfaces for the small TIM chaperone complexes within the core TIM22 components (Fig. 2B). TIM29 has a large C-terminal IMS domain which is capable of making contacts with TOM40 [21]. Both TIM10 and TIM9 crosslinked to a specific region (between AA 210–220) within this IMS domain, alluding to a possible binding site for the small TIM chaperones that may help guide an incoming precursor from the TOM complex to the TIM22 insertion site.

Additional crosslinks were detected between the small TIM chaperone complex and TIM22. The TIM22 binding site for small TIMs seems to narrow to an IMS facing helical region, just prior to the first TM domain (AA 55–64). This conformation suggests a chaperone docking site positioned close to the membrane interface of TIM22, which could poise the precursor protein ready for insertion into the TIM22 pore. Interestingly, the recently identified TIM22^{V33L} disease-causing mutation [33] is also located adjacent to this helical IMS region and may therefore interfere with the binding of the chaperone complex to TIM22.

Several crosslinks were also identified between the small TIM chaperones and AGK. AGK catalyses the ATP-dependent phosphorylation of monoacylglycerol or diacylglycerol to lysophosphatidyl acid (LPA) or phosphatidic acid (PA) respectively and although it has been shown to be a functional and stoichiometric constituent of TIM22, its role within the complex has remained unknown [22,23]. Intriguingly, both TIM9 and TIM10 formed crosslinks within the kinase domain of AGK, suggesting that the kinase domain may also function as a docking site for the small TIM hexamers. It was previously concluded that the function of AGK for TIM22 import is independent of its kinase function, based on the observation that kinase-dead AGK mutants do not have a defect in TIM22

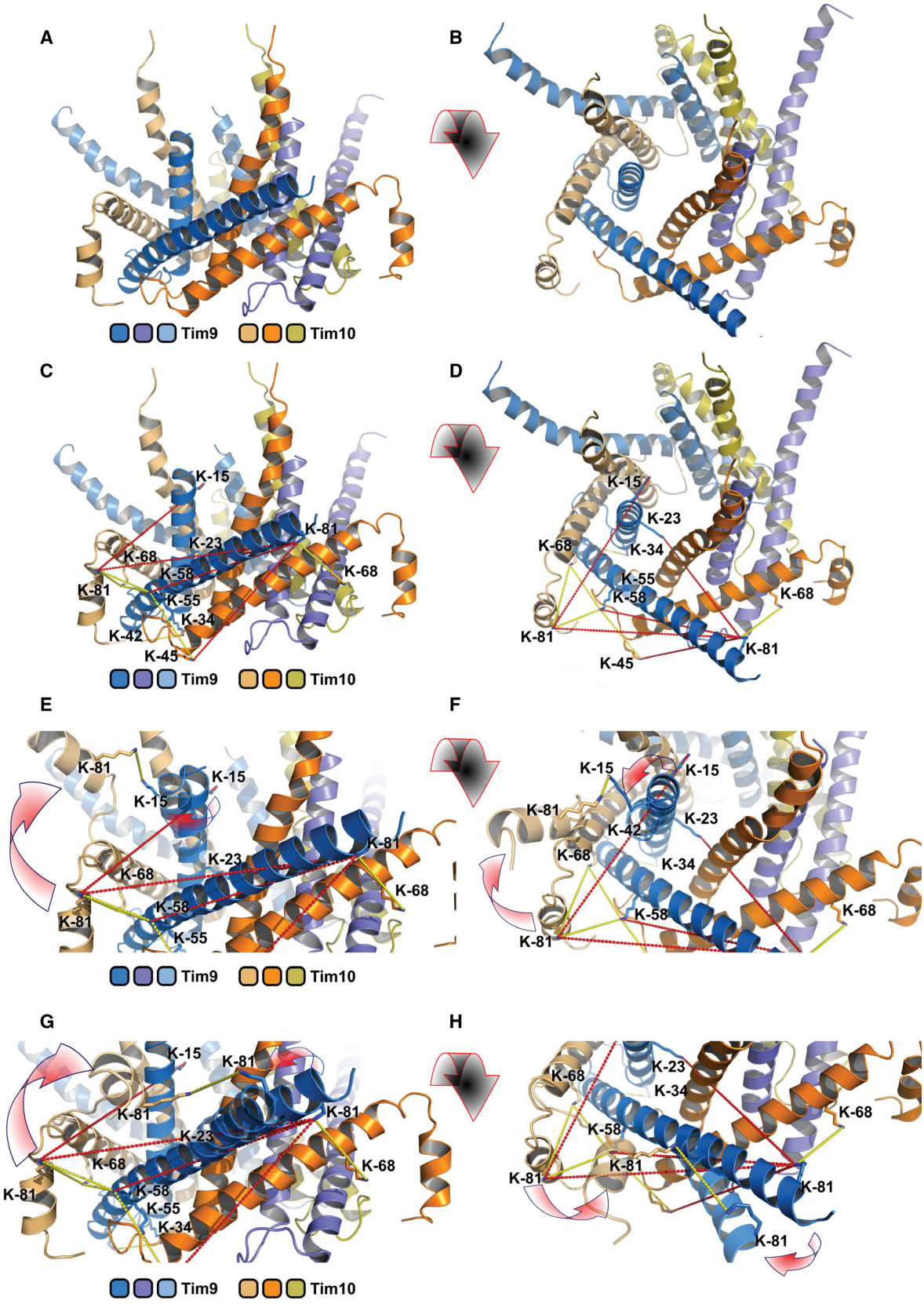
A
B
Tim9
Tim10
C
K-15
K-81
K-23
K-68
K-58
K-68
K-81
K-55
K-34
K-42
K-45
Tim9
Tim10
D
K-15
K-23
K-68
K-34
K-55
K-58
K-68
K-81
K-81
K-45
E
K-81
K-15
K-15
K-81
K-23
K-68
K-68
K-58
K-81
K-55
Tim9
Tim10
F
K-15
K-15
K-81
K-23
K-42
K-68
K-34
K-58
K-68
K-81
G
K-15
K-81
K-81
K-81
K-23
K-68
K-68
K-81
K-58
K-55
K-34
Tim9
Tim10
H
K-68
K-23
K-34
K-68
K-58
K-81
K-81
K-81
K-81

Fig. 3. Crosslinks demonstrate conformational flexibility within the TIM9-TIM10 chaperone complex. (A) Model of the TIM9-TIM10 hexameric chaperone complex based on the crystal structure (PDB id:2BSK). Fragments of missing N or C termini were modelled (extended) based on the best resolved copy of Tim9 or Tim10 subunit in this structure. The completed model was refined in ROSETTA using the relax option (constraints to the starting coordinates have been applied), and missing side chain atoms in the deposited crystal structure were generated in order to visualize x-links (several Lys residues). (B) Orthogonal view of (A). (C) Crosslinks modelled onto (A). Crosslinks that are complicit with the distance of the 11.4 Å arm length of the BS3 crosslinker are shown in yellow, and crosslinks that do not comply are shown in red. (D) Orthogonal view of (C). (E) Model based on (C) showing the conformational change required for the TIM9 Lys15 – TIM10 Lys81 crosslink to fulfil the spatial criteria. Red arrows indicate the conformational changes in the helices. (F) Orthogonal view of (E). (G) Model based on (C) showing the conformational change required for the TIM9 Lys81 – TIM10 Lys81 crosslink to fulfil the spatial criteria. Red arrows indicate the conformational changes in the helices. (H) Orthogonal view of (G).

stability or import [22,23]. However, the observation in this study that the small TIM chaperones interact closely with the kinase domain, may allude to some coordination between lipid kinase function and TIM22 import. Additional functional studies are required to investigate this further.

The TIM10B protein was suggested to be a homolog of the yeast Tim12 which serves as a docking site for the small TIM chaperones [28,29]. Only one crosslink was detected between TIM10B (K55) and TIM9 (K81), suggesting that it does indeed interact with the small TIM complex. However, this crosslink was only detected in one of the XL-MS experimental replicates and the lack of additional crosslinking data for this protein prevents any meaningful modelling.

2Although it is possible that these crosslinks reflect a single chaperone binding pocket that contacts each of TIM29, TIM22 and AGK, it is more likely that these multiple binding regions are indicative of docking sites for multiple TIM chaperone complexes. Analysis of TIM22 precursor-chaperone complexes from yeast identified at least two chaperone complexes per precursor and that the stoichiometry was dependent on precursor length [9]. These hexamers form a clamp-like hold on the precursor to maintain it in an elongated conformation. A tight binding of the hexamers to the precursor is retained until its release into the TIM22 channel [9]. Based on this model, the translocase would be expected to accommodate multiple small TIM hexamers. The multiple chaperone binding sites uncovered by these crosslinking experiments are consistent with a similar mechanism occurring in human. Since the IMS domain of TIM29 can connect with TOM40, the binding of a small TIM hexamer within this region could represent the first contact point for incoming precursor-chaperone complexes with the core complex. This 'handover' step would then facilitate shuttling of the precursor-chaperone complex from the TOM complex to the insertion site of TIM22. The identified small TIM binding site on the N-terminal region of TIM22 is just prior to the first TM and therefore an ideal position for release of the precursor into the channel. The role of AGK in this model remains to be determined. It could represent a third binding site, or it could be part of the binding site with TIM22.

While this manuscript was in the submission process, a cryo-EM structure of the human TIM22 complex was published at a resolution of 3.7 Å [56]. This structure was derived from cells overexpressing the individual components of the TIM22 complex. However, certain aspects of this structure could be considered contentious, including the lack of a twin pore, which had previously been shown, using both cryo-EM and electrophysiology studies, to be an essential feature of the yeast TIM22 complex [12,13]. It therefore also remains unclear whether this structure represents the functional TIM22 complex or an intermediate. Nevertheless, in agreement with the notion that multiple TIM hexamers can dock at the complex, the cryo-EM model depicts two small TIM hexamers, one consisting of TIM9-TIM10-TIM10B situated onto the N terminus of TIM22, and the other comprising of TIM9-TIM10, which is stabilized by the C-terminal IMS region of TIM29 [56]. AGK was also shown to interact with the TIM9-TIM10-TIM10B hexamer, whereby N94 within the kinase domain can form a hydrogen bond with R39 in TIM9 [56]. Due to a lack of electron density, the matrix N-terminal portion of TIM29 was poorly resolved in the Cryo-EM model [56]. Using XL-MS, we identify contacts of this N-terminal segment with the first matrix loop of TIM22, close to the second TM domain. Therefore, our XL-MS data set is a valuable complementation to the recently published TIM22 structure, verifying interactions that are present in the natively isolated complex and providing further spatial definition for crosslinked residues.

Conclusion

Recent years have brought about significant advancements in understanding the composition of the human

TIM22 complex. However structural information on complex arrangement is still lacking. By developing a strategy for large scale isolation of sufficiently pure TIM22 complex, we were able to undertake a XL-MS approach to better understand its molecular architecture. The crosslinking data generated have uncovered several key structural features of the complex. The matrix domains of TIM29 and TIM22 are in close proximity, indicating these regions could be important for complex stability. The tentacles of the small TIM proteins in human, made up of the N and C termini of TIM9 and TIM10, are highly flexible, supporting this observation which has previously been observed in the yeast small TIM complex. Finally, chaperone complex contact sites within TIM29, TIM22 and AGK indicate that the small TIM chaperones have multiple docking sites within the core complex.

These novel insights raise several interesting questions: what is the function of each of these chaperone binding sites? Does precursor transfer involve sequential binding of the small TIMs, or simultaneous binding of multiple small TIM chaperones? The role of small TIM binding to the kinase domain of AGK is a particularly compelling question and may help to elucidate the molecular function of AGK at the complex. Functional verification of these crosslinking sites is required to further unravel the steps that lead to TIM22-mediated translocation.

Acknowledgements

We thank Olaf Bernhard and Monika Rabe for their help in MS analysis. This work was supported by the Deutsche Forschungsgemeinschaft [SFB1190 (HU and PR); SFB860 (RF); EXC 2067/1-390729940] and by the Max Planck Society (HU and PR).

Author contributions

PR designed the project; SC, MD, RF, HU and AL designed experiments and evaluated the data; AV, AL, PN and SC performed experiments and analysed data. SC and PR wrote the paper with the input of other authors.

References

1 Gomkale R, Cruz-Zaragoza LD, Suppanz I, Guiard B, Montoya J, Callegari S, Pacheu-Grau D, Warscheid B and Rehling P (2020) Defining the substrate spectrum of the TIM22 complex identifies pyruvate carrier subunits as unconventional cargos. *Curr Biol* **30**, 1119–1127.e5.

2 Rampelt H, Sucec I, Bersch B, Horten P, Perschil I, Martinou J-C, van der Laan M, Wiedemann N, Schanda P and Pfanner N (2020) The mitochondrial carrier pathway transports non-canonical substrates with an odd number of transmembrane segments. *BMC Biol* **18**, 2.

3 Horten P, Colina-Tenorio L and Rampelt H (2020) Biogenesis of mitochondrial metabolite carriers. *Biomolecules* **10**, 1008.

4 Backes S, Hess S, Boos F, Woellhaf MW, Godel S, Jung M, Muhlhaus T and Herrmann JM (2018) Tom70 enhances mitochondrial preprotein import efficiency by binding to internal targeting sequences. *J Cell Biol* **217**, 1369–1382.

5 Brix J, Dietmeier K and Pfanner N (1997) Differential recognition of preproteins by the purified cytosolic domains of the mitochondrial import receptors Tom20, Tom22, and Tom70. *J Biol Chem* **272**, 20730–20735.

6 Brix J, Rudiger S, Bukau B, Schneider-Mergener J and Pfanner N (1999) Distribution of binding sequences for the mitochondrial import receptors Tom20, Tom22, and Tom70 in a presequence-carrying preprotein and a non-cleavable preprotein. *J Biol Chem* **274**, 16522–16530.

7 Sollner T, Pfaller R, Griffiths G, Pfanner N and Neupert W (1990) A mitochondrial import receptor for the ADP/ATP carrier. *Cell* **62**, 107–115.

8 Steger HF, Söllner T, Kiebler M, Dietmeier KA, Pfaller R, Trülzsch KS, Tropschug M, Neupert W and Pfanner N (1990) Import of ADP/ATP carrier into mitochondria: two receptors act in parallel. *J Cell Biol* **111**, 2353–2363.

9 Weinhäupl K, Lindau C, Hessel A, Wang Y, Schütze C, Jores T, Melchionda L, Schönfisch B, Kalbacher H, Bersch B *et al.* (2018) Structural basis of membrane protein chaperoning through the mitochondrial intermembrane space. *Cell* **175**, 1365–1379.e25.

10 Endres M, Neupert W and Brunner M (1999) Transport of the ADP/ATP carrier of mitochondria from the TOM complex to the TIM22.54 complex. *EMBO J* **18**, 3214–3221.

11 Koehler CM, Jarosch E, Tokatlidis K, Schmid K, Schweyen RJ and Schatz G (1998) Import of mitochondrial carriers mediated by essential proteins of the intermembrane space. *Science* **279**, 369–373.

12 Rehling P, Model K, Brandner K, Kovermann P, Sickmann A, Meyer HE, Kühlbrandt W, Wagner R, Truscott KN and Pfanner N (2003) Protein insertion into the mitochondrial inner membrane by a twin-pore translocase. *Science* **299**, 1747–1751.

13 Kovermann P, Truscott KN, Guiard B, Rehling P, Sepuri NB, Müller H, Jensen RE, Wagner R and Pfanner N (2002) Tim22, the essential core of the mitochondrial protein insertion complex, forms a voltage-activated and signal-gated channel. *Mol Cell* **9**, 363–373.

14 Sirrenberg C, Bauer MF, Guiard B, Neupert W and Brunner M (1996) Import of carrier proteins into the mitochondrial inner membrane mediated by Tim22. *Nature* **384**, 582–585.
15 Gebert N, Gebert M, Oeljeklaus S, von der Malsburg K, Stroud DA, Kulawiak B, Wirth C, Zahedi RP, Dolezal P, Wiese S *et al.* (2011) Dual function of Sdh3 in the respiratory chain and TIM22 protein translocase of the mitochondrial inner membrane. *Mol Cell* **44**, 811–818.
16 Hwang DK, Claypool SM, Leuenberger D, Tienson HL and Koehler CM (2007) Tim54p connects inner membrane assembly and proteolytic pathways in the mitochondrion. *J Cell Biol* **178**, 1161–1175.
17 Koehler CM, Murphy MP, Bally NA, Leuenberger D, Oppliger W, Dolfini L, Junne T, Schatz G and Or E (2000) Tim18p, a new subunit of the TIM22 complex that mediates insertion of imported proteins into the yeast mitochondrial inner membrane. *Mol Cell Biol* **20**, 1187–1193.
18 Kerscher O, Sepuri NB and Jensen RE (2000) Tim18p is a new component of the Tim54p-Tim22p translocon in the mitochondrial inner membrane. *Mol Biol Cell* **11**, 103–116.
19 Kerscher O, Holder J, Srinivasan M, Leung RS and Jensen RE (1997) The Tim54p-Tim22p complex mediates insertion of proteins into the mitochondrial inner membrane. *J Cell Biol* **139**, 1663–1675.
20 Callegari S, Richter F, Chojnacka K, Jans DC, Lorenzi I, Pacheu-Grau D, Jakobs S, Lenz C, Urlaub H, Dudek J *et al.* (2016) TIM29 is a subunit of the human carrier translocase required for protein transport. *FEBS Lett* **590**, 4147–4158.
21 Kang Y, Baker MJ, Liem M, Louber J, McKenzie M, Atukorala I, Ang C-S, Keerthikumar S, Mathivanan S and Stojanovski D (2016) Tim29 is a novel subunit of the human TIM22 translocase and is involved in complex assembly and stability. *Elife* **5**, e17463.
22 Kang Y, Stroud DA, Baker MJ, De Souza DP, Frazier AE, Liem M, Tull D, Mathivanan S, McConville MJ, Thorburn DR *et al.* (2017) Sengers syndrome-associated mitochondrial acylglycerol kinase is a subunit of the human TIM22 protein import complex. *Mol Cell* **67**, 457–470.e5.
23 Vukotic M, Nolte H, Konig T, Saita S, Ananjew M, Kruger M, Tatsuta T and Langer T (2017) Acylglycerol kinase mutated in Sengers syndrome is a subunit of the TIM22 protein translocase in mitochondria. *Mol Cell* **67**, 471–483.e7.
24 Wrobel L, Sokol AM, Chojnacka M and Chacinska A (2016) The presence of disulfide bonds reveals an evolutionarily conserved mechanism involved in mitochondrial protein translocase assembly. *Sci Rep* **6**, 27484.
25 Bauer MF, Rothbauer U, Muhlenbein N, Smith RJ, Gerbitz K, Neupert W, Brunner M and Hofmann S (1999) The mitochondrial TIM22 preprotein translocase is highly conserved throughout the eukaryotic kingdom. *FEBS Lett* **464**, 41–47.
26 Paschen SA, Rothbauer U, Kaldi K, Bauer MF, Neupert W and Brunner M (2000) The role of the TIM8-13 complex in the import of Tim23 into mitochondria. *EMBO J* **19**, 6392–6400.
27 Curran SP, Leuenberger D, Schmidt E and Koehler CM (2002) The role of the Tim8p-Tim13p complex in a conserved import pathway for mitochondrial polytopic inner membrane proteins. *J Cell Biol* **158**, 1017–1027.
28 Adam A, Endres M, Sirrenberg C, Lottspeich F, Neupert W and Brunner M (1999) Tim9, a new component of the TIM22.54 translocase in mitochondria. *EMBO J* **18**, 313–319.
29 Wagner K, Gebert N, Guiard B, Brandner K, Truscott KN, Wiedemann N, Pfanner N and Rehling P (2008) The assembly pathway of the mitochondrial carrier translocase involves four preprotein translocases. *Mol Cell Biol* **28**, 4251–4260.
30 Kang Y, Anderson AJ, Jackson TD, Palmer CS, De Souza DP, Fujihara KM, Stait T, Frazier AE, Clemons NJ, Tull D *et al.* (2019) Function of hTim8a in complex IV assembly in neuronal cells provides insight into pathomechanism underlying Mohr-Tranebjaerg syndrome. *Elife* **8**, e48828.
31 Muhlenbein N, Hofmann S, Rothbauer U and Bauer MF (2004) Organization and function of the small Tim complexes acting along the import pathway of metabolite carriers into mammalian mitochondria. *J Biol Chem* **279**, 13540–13546.
32 Webb CT, Gorman MA, Lazarou M, Ryan MT and Gulbis JM (2006) Crystal structure of the mitochondrial chaperone TIM9.10 reveals a six-bladed alpha-propeller. *Mol Cell* **21**, 123–133.
33 Pacheu-Grau D, Callegari S, Emperador S, Thompson K, Aich A, Topol SE, Spencer EG, McFarland R, Ruiz-Pesini E, Torkamani A *et al.* (2018) Mutations of the mitochondrial carrier translocase channel subunit TIM22 cause early-onset mitochondrial myopathy. *Hum Mol Genet* **27**, 4135–4144.
34 Calvo SE, Compton AG, Hershman SG, Lim SC, Lieber DS, Tucker EJ, Laskowski A, Garone C, Liu S, Jaffe DB *et al.* (2012) Molecular diagnosis of infantile mitochondrial disease with targeted next-generation sequencing. *Sci Transl Med* **4**, 118ra10.
35 Siriwardena K, MacKay N, Levandovskiy V, Blaser S, Raiman J, Kantor PF, Ackerley C, Robinson BH, Schulze A and Cameron JM (2013) Mitochondrial citrate synthase crystals: novel finding in Sengers syndrome caused by acylglycerol kinase (AGK) mutations. *Mol Genet Metab* **108**, 40–50.
36 Haghighi A, Haack TB, Atiq M, Mottaghi H, Haghighi-Kakhki H, Bashir RA, Ahting U, Feichtinger RG, Mayr JA, Rötig A *et al.* (2014) Sengers syndrome: six novel AGK mutations in seven new families and

review of the phenotypic and mutational spectrum of 29 patients. *Orphanet J Rare Dis* **9**, 119.
37 Mayr JA, Haack TB, Graf E, Zimmermann FA, Wieland T, Haberberger B, Superti-Furga A, Kirschner J, Steinmann B, Baumgartner MR *et al.* (2012) Lack of the mitochondrial protein acylglycerol kinase causes Sengers syndrome. *Am J Hum Genet* **90**, 314–320.
38 Roesch K, Curran SP, Tranebjaerg L and Koehler CM (2002) Human deafness dystonia syndrome is caused by a defect in assembly of the DDP1/TIMM8a-TIMM13 complex. *Hum Mol Genet* **11**, 477–486.
39 Jin H, May M, Tranebjærg L, Kendall E, Fontán G, Jackson J, Subramony Sh, Arena F, Lubs H, Smith S *et al.* (1996) A novel X-linked gene, DDP, shows mutations in families with deafness (DFN-1), dystonia, mental deficiency and blindness. *Nat Genet* **14**, 177–180.
40 Callegari S, Müller T, Schulz C, Lenz C, Jans DC, Wissel M, Opazo F, Rizzoli SO, Jakobs S, Urlaub H *et al.* (2019) A MICOS-TIM22 association promotes carrier import into human mitochondria. *J Mol Biol* **431**, 2835–2851.
41 Mohanraj K, Wasilewski M, Benincá C, Cysewski D, Poznanski J, Sakowska P, Bugajska Z, Deckers M, Dennerlein S, Fernandez-Vizarra E *et al.* (2019) Inhibition of proteasome rescues a pathogenic variant of respiratory chain assembly factor COA7. *EMBO Mol Med* **11**, e9561.
42 Hughes CS, Foehr S, Garfield DA, Furlong EE, Steinmetz LM and Krijgsveld J (2014) Ultrasensitive proteome analysis using paramagnetic bead technology. *Mol Syst Biol* **10**, 757.
43 Moggridge S, Sorensen PH, Morin GB and Hughes CS (2018) Extending the compatibility of the SP3 paramagnetic bead processing approach for proteomics. *J Proteome Res* **17**, 1730–1740.
44 Leitner A, Reischl R, Walzthoeni T, Herzog F, Bohn S, Forster F and Aebersold R (2012) Expanding the chemical cross-linking toolbox by the use of multiple proteases and enrichment by size exclusion chromatography. *Mol Cell Proteomics* **11**, M111.014126.
45 Chen Z-L, Meng J-M, Cao Y, Yin J-L, Fang R-Q, Fan S-B, Liu C, Zeng W-F, Ding Y-H, Tan D *et al.* (2019) A high-speed search engine pLink 2 with systematic evaluation for proteome-scale identification of cross-linked peptides. *Nat Commun* **10**, 3404.
46 Cox J and Mann M (2008) MaxQuant enables high peptide identification rates, individualized p.p.b.-range mass accuracies and proteome-wide protein quantification. *Nat Biotechnol* **26**, 1367–1372.
47 Combe CW, Fischer L and Rappsilber J (2015) xiNET: cross-link network maps with residue resolution. *Mol Cell Proteomics* **14**, 1137–1147.
48 Emsley P, Lohkamp B, Scott WG and Cowtan K (2010) Features and development of Coot. *Acta Crystallogr D Biol Crystallogr* **66**, 486–501.
49 Nivon LG, Moretti R and Baker D (2013) A Pareto-optimal refinement method for protein design scaffolds. *PLoS One* **8**, e59004.
50 Shiota T, Imai K, Qiu J, Hewitt Vl, Tan K, Shen H-h, Sakiyama N, Fukasawa Y, Hayat S, Kamiya M *et al.* (2015) Molecular architecture of the active mitochondrial protein gate. *Science* **349**, 1544–1548.
51 Spahr H, Rozanska A, Li X, Atanassov I, Lightowlers RN, Chrzanowska-Lightowlers ZM, Rackham O and Larsson NG (2016) SLIRP stabilizes LRPPRC via an RRM-PPR protein interface. *Nucleic Acids Res* **44**, 6868–6882.
52 Sasarman F, Brunel-Guitton C, Antonicka H, Wai T, Shoubridge EA and LSFC Consortium (2010) LRPPRC and SLIRP interact in a ribonucleoprotein complex that regulates posttranscriptional gene expression in mitochondria. *Mol Biol Cell* **21**, 1315–1323.
53 Linden A, Deckers M, Parfentev I, Pflanz R, Homberg B, Neumann P, Ficner R, Rehling P and Urlaub H (2020) A cross-linking mass spectrometry approach defines protein interactions in yeast mitochondria. *Mol Cell Proteomics* **19**, 1161–1178.
54 Kumar A, Matta SK and D'Silva P (2020) Conserved regions of budding yeast Tim22 have a role in structural organization of the carrier translocase. *J Cell Sci* **133**.
55 Baker MJ, Webb CT, Stroud DA, Palmer CS, Frazier AE, Guiard B, Chacinska A, Gulbis JM and Ryan MT (2009) Structural and functional requirements for activity of the Tim9-Tim10 complex in mitochondrial protein import. *Mol Biol Cell* **20**, 769–779.
56 Qi L, Wang Q, Guan Z, Wu Y, Shen C, Hong S, Cao J, Zhang X, Yan C and Yin P (2020) Cryo-EM structure of the human mitochondrial translocase TIM22 complex. *Cell Res*. https://doi.org/10.1038/s41422-020-00400-w. [Epub ahead of print].

Supporting information

Additional supporting information may be found online in the Supporting Information section at the end of the article.

Fig. S1. Volcano plot depicting the Label Free Quantification (LFQ) intensity (Log2 scale) for proteins identified through mass spectrometry analysis after TIM22 complex isolation without RNase A treatment (X-axis) and with RNase A treatment (Y-axis).

Fig. S2. Superimposition of *S. cerevisiae* small TIM chaperone complex on human complex.

Table S1. Mass spectrometry analysis of the BS3 x-linked TIM29 complex components